Vol.23, No.4, PP.76-86 P-ISSN: 2070-4003 E-ISSN: 2664-5548

# Mathematical Modeling of Whispering Gallery Mode Resonators for High-Sensitivity Refractive Index Sensing

## Farah A. Lazem<sup>1,2</sup>\*, Haider Y. Hammod<sup>1</sup>, and Aseel I. Mahmood<sup>3</sup>

<sup>1</sup>Department of Physics, College of Science for Women, University of Baghdad, Baghdad, Iraq

<sup>2</sup>College of Science, AL-Karkh University of Science, Baghdad, Iraq

<sup>3</sup>Scientific Research Commission, Ministry of Higher Education and Scientific Research, Baghdad, Iraq

<sup>a\*</sup>Corresponding author: farah.lazem1204@sc.uobaghdad.edu.iq

#### **Abstract**

In this study, the Single-Mode Fiber (SMF) was examined in a theoretical investigation of the impact of the medium on the two Whispering Gallery Mode Resonator (WGMR) models using MATLAB software. It was found that the Free Spectral Range (FSR) has an inverse relationship with the resonator radius, and it was equal to 0.33 THz. The low FSR value is caused by the big microsphere resonator. A high Q-factor is defined as 0.175 x 10<sup>5</sup>. The resonance spectrum was found to diminish when the surrounding media's refractive index rose. The WGMR's evanescent field interacts with the external medium more strongly when the surrounding environment's refractive index increases. The resonant modes' boundary conditions were altered by this interaction, which raises the modes' effective refractive index. The WGMR resonance frequency may also shift as a result of changes in the surrounding medium refractive index. To achieve highresolution sensing, the surrounding medium of the spherically shaped WGMR was altered at a step of 0.002 in the range of 1.33 to 1.35. As for the sensitivity value, a value of (-) 100.152 THz/RIU was obtained, which is considered a good value for use as a sensor.

#### Article Info.

#### **Keywords:**

Whispering Gallery Mode, Free Spectral Range, Quality Factor, Evanescent Field, Single Mode Fiber.

#### **Article history:**

Received: Feb. 12, 2025 Revised: Apr. 25, 2025 Accepted: May, 12, 2025 Published: Dec. 01, 2025

## 1. Introduction

Optical Whispering Gallery Mode Resonators (WGMRs) have intrinsic benefits as sensing devices. WGMR sensors have a substantially smaller device footprint than interferometric sensors because the interferometric arm is "folded" into the roundtrip pass. Furthermore, high-finesse microcavities enable light to interact with the analytes or targets of interest millions of times due to light performing numerous round-trips in the same mode volume, thereby increasing the sensitivity of the sensors [1]. This results in a significantly lower device size. Furthermore, since the light performs numerous round excursions in the same volume of mode, that is why WGMR is one of the most important optical sensors, attracting many researchers due to its numerous uses [2]. They got their name from a phenomenon found in London's St. Paul's Cathedral. Because sound waves bounce off the gallery's round wall one after the other, whispers can be heard inside the cathedral along the dome's curved wall [3]. Optical WGMRs limit the light inside tiny buildings via total internal reflection phenomenon, with resonant light circling millions of times as sound does in St. Paul's Cathedral [4]. The ultrahigh quality factor (Q), the comparatively tiny mode volume, and the variety of geometries and materials available for WGMRs have resulted in significant breakthroughs in the field of WGMR-based optical sensing [5]. Whispering Gallery Modes (WGMs) are patterns of electromagnetic waves (typically optical or microwave) that are trapped within circular or quasi-circular structures (such as spheres, disks, or toroid's) and travel along their perimeter via total internal reflection [6].

<sup>© 2025</sup> The Author(s). Published by College of Science, University of Baghdad. This is an open-access article distributed under the terms of the Creative Commons Attribution 4.0 International License (<a href="https://creativecommons.org/licenses/by/4.0/">https://creativecommons.org/licenses/by/4.0/</a>).

WGMR's distinctive qualities include: High Q-factor: very good resonance quality (means less energy loss), high sensitivity to environmental changes (temperature, refractive index, etc.), wavelength selectivity: the ability to accurately discern between distinct wavelengths, small size: can be made at the micro- or even nano-scale. Both types of fiber as single-mode fiber (SMF) and multimode fiber (MMF) fiber (Single-Mode/Multi-Mode/Single-Mode) (SMS) can be used [7]. A Single-Mode/Multi-Mode/Single-Mode (SMS) fibers structure consists of a small segment of Multimode Fiber (MMF) spliced between two single-mode fibers. SMS structures are often referred to as fiber heterostructures, as they typically include a variety of fiber kinds [8]. SMF structures provide advantages, such as simplicity of manufacture, low cost, variable design, and high sensitivity, making them helpful for developing real-world sensors [9]. We discuss some previous research conducted on the topic of WGMR using SMF.

A previous study focused on the design and development of a highly sensitive optical displacement sensor built on a U-shaped curved SMS (Single-Mode/MultiMode/Single-Mode) optical fiber structure. The sensor measured fine displacements with a sensitivity of up to 34.46 nm/μm in a narrow displacement range. A mathematical model was presented using MATLAB. WGMR was designed using SMF as delivery fiber of diameter 1 μm and resonator fiber with a spherical shape of radius 100 μm[10]. Studies have been done on an optical sensor that uses chemically etched single-mode optical fibers to detect surface plasmon resonance (SPR) events. They attained a sensitivity of up to 3800 nm/RIU in reflection mode, and 5100 nm/RIU in transmission mode. This falls within the refractive index range of 1.33 to 1.37 [11]. Another study investigated and analyzed optical WGMR in a silicon sphere with a radius of 500 micrometers. The optical modes had high-quality factors, with a Q-factor of 10<sup>5</sup> measured at 1472 nanometers [12].

In this work, MATLAB was used to build a mathematical model to evaluate the performance of WGMR as a refractive index sensor by changing the medium surrounding the WGMR.

## 2. The Mathematical Model

In the frequency domains of electric and magnetic-optical fields, the two-dimensional system utilizes Maxwell's homogeneous equations E and H [13]:

$$\nabla \times \mathbf{H} - i\omega \epsilon_0 \epsilon \mathbf{E} = 0 , \qquad -\nabla \times \mathbf{E} - i\omega \mu_0 \mathbf{H} = 0$$
 (1)

where the Eigen frequency is denoted by  $\omega$ , the electric permittivity in a material by  $\varepsilon$ , and the magnetic permeability and electric permittivity in free space by  $\varepsilon_0$  and  $\mu_0$ , respectively. For the vacuum speed of light c, the stationary fields oscillate at  $\sim e^{i\omega t}$  in time with the real excitation frequency  $\omega = 2\pi c/\lambda$ , which is determined by the wavelength  $\lambda$ .

Quality-Factor  $(Q_F)$  is a key factor in the explanation of photon temporal confinement and microresonators. The intracavity energy W exhibits exponential decline when light travels through microcavities [13]:

$$W(t) = W_0 e^{-t/\tau}$$
 (2)

where  $W_o$  and  $\tau$  stand for the photon lifetime and starting energy, respectively. The quality-factor  $Q_F$  is defined as the ratio of the intracavity stored energy to the energy loss rate [13]:

rate [13]:  

$$Q_{F} = \omega_{m} \frac{W}{-dW/dt}$$
(3)

where  $\omega_{\rm m}$  is the resonance angular frequency. After one oscillation period  $T=1/\nu$ , he energy turns into:

$$W = W_0 e^{-1/\tau v} \tag{4}$$

According to the definition of  $Q_F$  [14]:

$$Q_{F} = 2\pi \frac{\text{stored energy}}{\text{energy loss per oscillation period}} = 2\pi \frac{1}{1 - e^{-1/\tau v}}$$
 (5)

If the optical signal energy oscillates and decays as  $e^{iwt}e^{-t/2\tau}$ , then [1]:

$$Q_F = \tau w = 2\pi v \tau = 2\pi c \tau / \lambda \tag{6}$$

The losses in microresonators mainly come from radiation  $(1/Q_{rad})$ , material  $(1/Q_{mat})$ , surface and bulk scattering  $(1/Q_{sca})$ , and coupling  $(1/Q_{coup})$ . These losses impact the mode linewidth and result in total Q given by [1, 13]:

$$\frac{1}{Q} = \frac{1}{Q_{\text{rad}}} + \frac{1}{Q_{\text{mat}}} + \frac{1}{Q_{\text{sca}}} + \frac{1}{Q_{\text{coup}}} + \dots$$
 (7)

Radiation loss is greatest in small resonators and is related to microcavity size. Material absorption loss increases with resonator size, and the host medium starts to limit the microcavities.  $Q_F$ , given by  $Q_{abs} = 2\pi n/\alpha \lambda m$ , where n represents the resonator's refractive index. and  $\alpha$  is the medium absorption coefficient. For instance, the ultimate material limited  $Q_F$  for a silica microsphere cavity is around  $10^{10}$  [2, 14].

Another basic parameter for describing the WGMR is the Free Spectral Range (FSR) which is defined as the distance between the two closest resonances, for not equidistant peaks FSR given by [15]:

$$FSR (vm) = v_{m+1} - v_m$$
 (8)

For equidistant peaks, assume  $nR_{Res.} \gg \lambda_m$  so FSR (vm) [15]:

$$FSR (vm) = \frac{c}{nR_{Res}}$$
 (9)

The finesse F is defined as (FSR, the frequency difference between neighboring resonant peaks) and the mode FWHM (Full Width at Half Maximum) [16]:

$$Finess = \frac{FSR}{FWHM} = \frac{\Delta\lambda}{\lambda} = \frac{\Delta v}{v}$$
 (10)

The  $Q_F$  could be describe due to Finess as [16]:

$$Q_{F} = \frac{2\pi n R_{Res.}}{\lambda} \text{ Finess} = \frac{2\pi n R_{Res.} v}{c} \text{ Finess}$$
 (11)

When the length of the light route loop L equals the wavelength in the optical structure, the  $Q_F$  equals the finesse. If the resonance is created by many wavelengths in the light path loop length, then the  $Q_F$  is greater than the finesse.

In this work, the MATLAB application was used to build the mathematical model for evaluating the performance of WGMR as a refractive index sensor. The parameters considered were the speed of light in vacuum equals 3 x 10<sup>8</sup> m/s and the laser frequency range 190-200 THz. The resonator was of spherical shape made from silica. The refractive index was set at 1.45. The resonator radius was chosen as 100 µm. The reason for selecting a large sphere radius is that it offers a high Q-factor. The delivery fiber was SMF made from silica and tapered to 1 µm to achieve optimum coupling with the resonator fiber. The final structure was a spherical-shaped WGMR. The surrounding medium of the WGMR was changed by applying liquids of different refractive indices (1.33-1.35). The Figure of Merit (FOM) is an essential parameter for evaluating optical sensor performance. A key contributor to the FOM of a sensor is its sensitivity (S) [17]:

$$S = \frac{\Delta \lambda_{\text{res}}}{\Delta RI}$$
 (12)

where  $\Delta \lambda_{res}$  is the difference in resonance wavelength, and  $\Delta RI$  is the variation in surrounding refractive index.

The FOM is a parameter that depends on the width of the resonance dip and how it is affected by the applied stimuli. Therefore, the FOM is defined [18, 19]:

$$FOM = \frac{S}{FWHM}$$
 (13)

where FWHM is the Full Width at Half-Maximum of the resonance dip. Assuming that a 0.1 nm change in the position of a mode can be detected reliably, the sensor resolution is *RES* [20]:

$$RES = \frac{0.1 \text{ nm}}{S}$$
 (14)

Finally, the degree of precision with which the angular position of the dip minimum in an SPR curve may be determined is known as Detection Accuracy (DA). The definition of the detection accuracy is expressed as [21]:

$$DA (THz^{-1}) = \frac{1}{FWHM}$$
 (15)

The simulation model solves the characteristic equations governing the formation of WGMRs in a dielectric microsphere under whispering gallery conditions. The interaction between the guided mode in the tapered delivery fiber and the microsphere resonator was modelled using coupled-mode theory. To assess the sensor's response to external refractive index changes, the surrounding medium of the resonator was varied across a range of refractive indices 1.332- 1.35 RIU, and the corresponding shifts in resonance frequencies were calculated. This approach allows the evaluation of the WGMR sensitivity as a Refractive Index (RI) sensor.

## 3. Results and Discussion

The FSR and Q-Factor of the selective mode were analyzed and calculated using Eqs. (9) and (6), respectively, as it is clear in Fig.1.

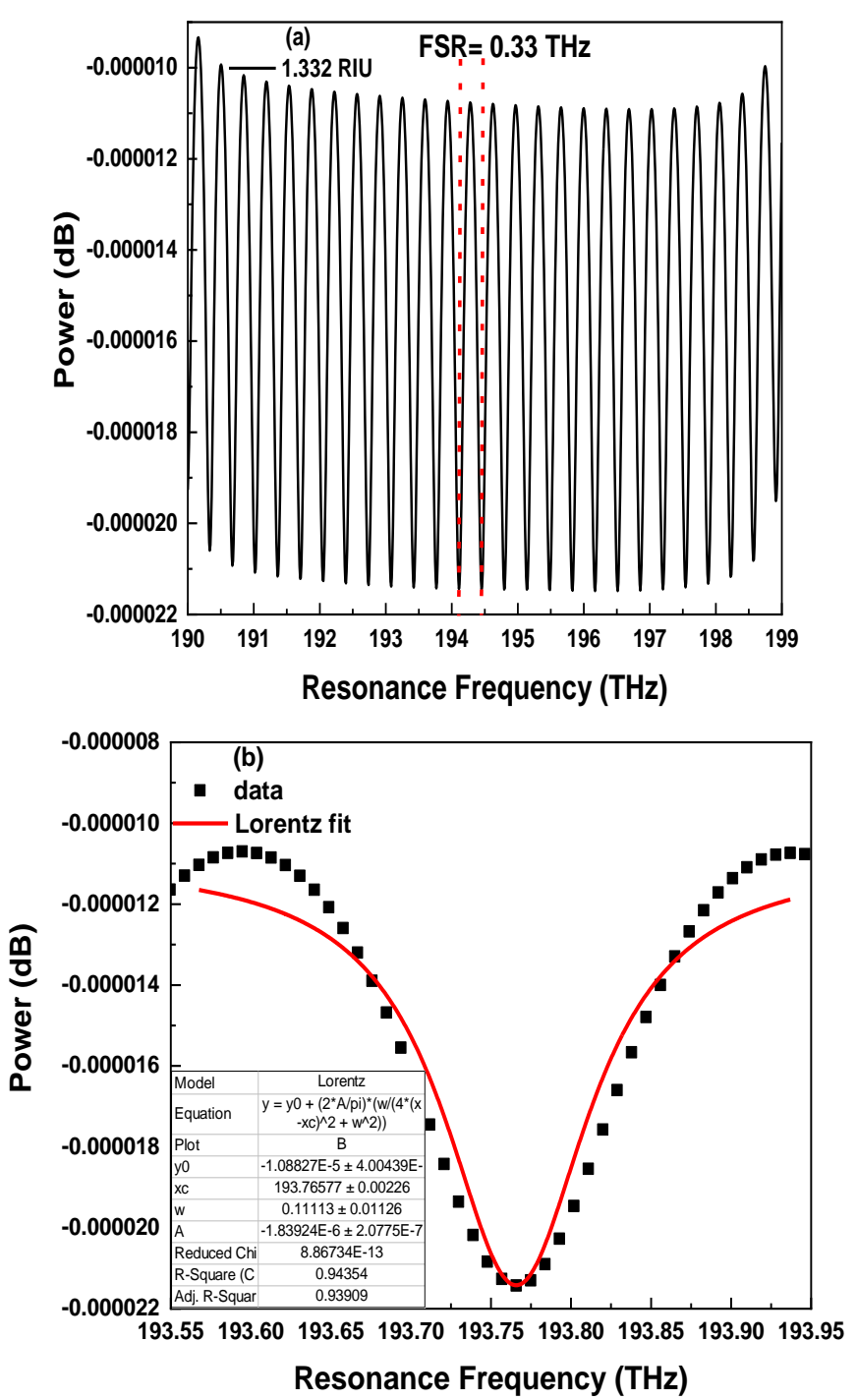


Figure 1: (a) FSR, and (b) Q-Factor of WGMR spectrum for a selected refractive index of 1.332.

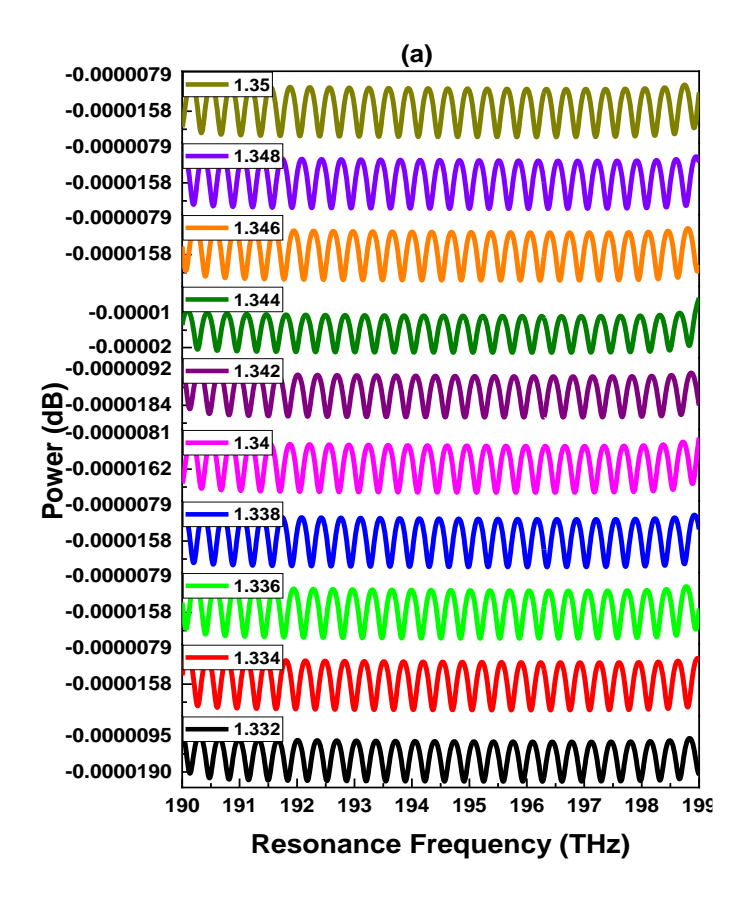
The FSR was inversely related to the resonator radius and was calculated to be 0.33 THz. The small value of FSR was due to the large microsphere resonator. The Q-factor was  $0.175 \times 10^5$ , which is considered high and good. The choice of resonator diameter plays a pivotal role in determining the spectral and confinement properties of WGMRs, particularly for sensing applications. The resonator radius of 100  $\mu$ m is

considered a moderate range, which balances the advantages offered by smaller and larger resonators. Moderate-sized resonators provide a compromise between FSR and mode volume, making them versatile for sensing applications. According to Eq. (9), as the radius of the resonator increases, the optical path length for one complete round-trip of the mode increases, leading to a denser mode distribution in the frequency domain. Consequently, larger resonators exhibit smaller FSR values [15].

The moderate diameters offer sufficient spectral spacing to differentiate adjacent modes while still supporting high Q-factors and efficient field confinement. This feature is critical in applications, such as biosensing and chemical sensing, where distinct resonance peaks are required for accurate measurements. Furthermore, the field confinement in moderate-sized resonators remains robust due to total internal reflection, resulting in reduced scattering losses compared to larger resonators. The mode volumes in this range are also sufficiently small to enhance light-matter interactions, a key factor for achieving high sensitivity in refractive index sensors [22].

The surrounding media of the designed spherical shape WGMR was changed in the range (1.332-1.35) with a step of 0.002 to get high-resolution sensing. The resonance spectra are illustrated in Fig 2.

As illustrated in Fig. 2, it is observed that when the refractive index of the surrounding media increased, the resonance spectrum decreased, and the evanescent field of the WGMR interacted more intensely with the external medium. This interaction changes the boundary conditions for the resonant modes, leading to an increase in the effective refractive index of the modes. Variations in the surrounding medium refractive index can also induce shifts in the WGMR resonance frequency, in addition to changes in the resonator material's size and refractive index brought on by temperature changes [23], which agrees with Eq.(11). The evanescent field of the WGM extends beyond the resonator surface, interacting with the surrounding medium. An increase in refractive index reduces the phase velocity of the propagating mode, effectively increasing the effective refractive index, which leads to a reduction in frequency. Besides high Q-factor, WGMRs have a significant fraction of their mode energy in the evanescent field. Small changes in the surrounding refractive index cause a proportionate change in the effective refractive index, making the resonator highly sensitive to environmental perturbations [24]. The sensitivity of the designed WGMR was calculated from the linear relationship between the resonance frequency and changing of surrounding refractive indices [25], as shown in Fig.3, where it was noticed that the higher the refractive index relative to the resonator, the lower the resonant frequency, i.e. an inverse relationship.



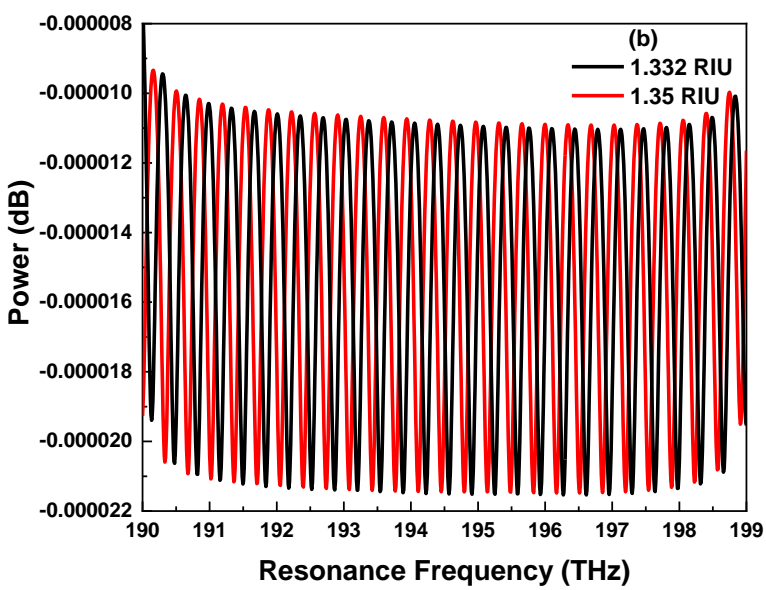


Figure 2: The resonance spectra for the spherical shape WGMR for (a) the whole range of refractive indices, and (b) the smallest (1.332 RIU) and the highest (1.35 RIU) refractive indices.

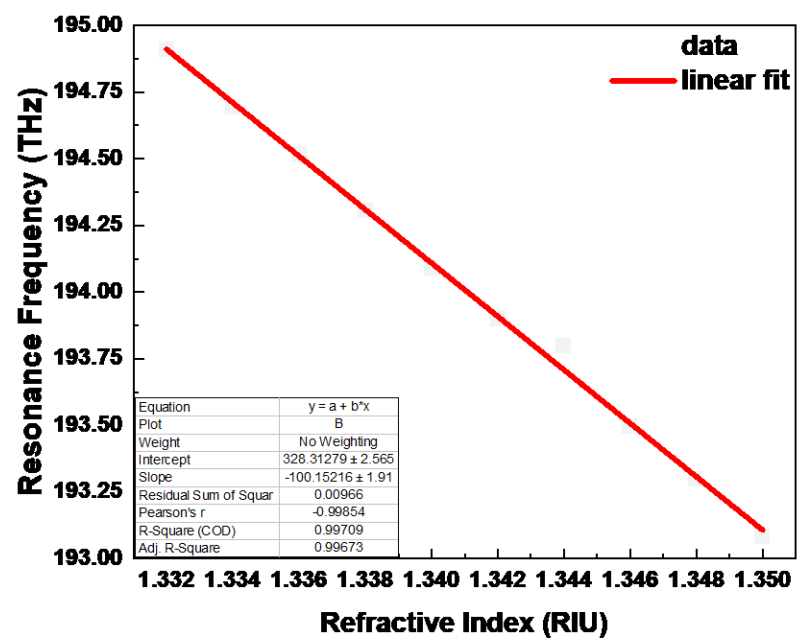


Figure 3: The relation between the resonance frequency and refractive index.

The figure of merit of the designed sensor is given in Table 1.

Table 1: The WGMR sensors parameters.

Sensitivity (THz/RIU)	Resolution (RIU)	FOM (RIU <sup>-1</sup> )	Q -Factor	FSR (THz)	Finess	DA (THz <sup>-1</sup> )
(-) 100.152	0.99X 10 <sup>-4</sup>	899.838	$0.175 \times 10^5$	0.33	2.972	9.009

According to Table 1, the sensor showed a high negative sensitivity, indicating a significant shift in resonance frequency per unit change in refractive index. The negative sign represents that the relationship between the resonance frequency and refractive index is inverse. Also, revised to a resolution of 10<sup>-4</sup>, the sensor can determine tiny changes in the refractive index, providing highly accurate detection of minute environmental changes. The high value of FOM reflects the efficiency of the sensor in delivering an effective resonance shift with minimal linewidth. The sensor's high Q-factor represents low energy losses and strong resonance confinement, allowing prolonged interaction between light and the surrounding medium, which is necessary for enhanced sensitivity and selectivity. The measured Q-factor fell within a practically relevant and accepted range for functional sensing platforms supporting the feasibility of the proposed device and agrees with others work [26]. The good finesse value indicates a suitable balance between the sensor's bandwidth and resonance sharpness, confirming precise frequency resolution and operational stability. Finally, the low detection limit shows the sensor's ability to measure extremely small resonance shifts. These performance metrics collectively indicate that the designed WGMR-RI sensor proved to be a robust and efficient tool for high-sensitivity refractive index sensing, with probable applications in environmental monitoring, biomedical diagnostics, and chemical detection. Table 2 illustrates a short comparison between the submitted work and others.

Table 2: Comparison with others works.

Sensor Type	Fabrication technique	Dlivery fiber diameter	Resonator Material and diameter	Q-Factor	Sensitivity	Ref.
Temperature	silica	SMF ,40	Silica, 47 µm	$5.54 \times 10^3$	25.5 pm/°C	[27]
	microsphere	μm			21.9 pm/°C	
	into an				•	
	embedded					
	dual-core					
	hollow fiber					
	EDCHF					
RI	Etched	SMF 18 µm	Silica, 122	$10^{4}$	Sucrose	[28]
	SMF,		μm		liquid (-) 83	
	Cylindrical				nm/RIU	
	Structure				Salty liquid	
					(-)74	
					nm/RIU	
This work	Simulation,	SMF-1µm	SMF-100 μm	0.175 x	(-) 100.152	This
	Etched SMF	,	·	$10^{5}$	THz/RIU	work
RI- sensor	Spherical					
KI SCHSOI	structure					

## 4. Conclusions

The presented study demonstrated the strong performance and versatility of the designed spherical WGMR. A notable advantage of this resonator configuration is its inherent tunability, wherein varying the microsphere diameter allows for precise control over key optical parameters, such as resonance frequency, quality factor, and free spectral range. Integrating an SMF as a delivery fiber mechanism enhances the overall system by enabling stable, efficient, and highly selective coupling to the resonator, thereby preserving sharp resonance features and achieving a high Q-factor. The developed SMF-WGMR sensor exhibited excellent refractive index sensing capabilities, achieving a Q-factor on the order of 10<sup>5</sup>, high sensitivity, and satisfactory resolution. These results highlight the potential of SMF-based spherical WGMRs in advanced optical sensing. Future work may explore alternative resonator geometries, materials, and coupling strategies to optimize performance further and expand application domains.

## **Conflict of Interest**

The authors declare that they have no conflict of interest.

#### References

- 1. N.M. Abas and A.A. Baqer, Baghdad Sci. J., 21, 1391, (2024). https://doi.org/10.21123/bsj.2023.8117.
- 2. A. Mahmood, V. Kavungal, S.S. Ahmed, G. Farrell, and Y. Semenova, Opt. Lett., **40**(41), 4983, (2015). https://doi.org/10.1364/OL.40.004983.
- 3. J. Barnes, G. Gagliardi, and H. Loock, Optica., 1(2), 75, (2014). https://doi.org/10.1364/OPTICA.1.000075.
- 4. L. Cai, J. Pan, Y. Zhao, J. Wang, and S. J. p. s. s. Xiao, Physica Status Solidi (a), **217**, 1900825, (2020). https://doi.org/10.1002/pssa.201900825.
- 5. M. Loyez, M. Adolphson, J. Liao, and L. Yang, ACS sensors, **8**(7), 2440, (2023). <a href="https://doi.org/10.1021/acssensors.2c02876">https://doi.org/10.1021/acssensors.2c02876</a>.
- 6. S. Yang, Y. Wang, and H. Sun, Adv. Opt. Mater., **3**(9), 1136, (2015). https://doi.org/10.1002/adom.201500232.
- 7. VA. E. Shitikov, I. A. Bilenko, N. M. Kondratiev, V. E. Lobanov, A. Markosyan, and M. L. Gorodetsky, Optica, **5**(12), 1525, (2018). <a href="https://doi.org/10.1364/OPTICA.5.001525">https://doi.org/10.1364/OPTICA.5.001525</a>.

- 8. G. Bernhard, and G. Seckmeyer, Atmos., **104**(D12), 14321 (1999). <a href="https://doi.org/10.1029/1999JD900180">https://doi.org/10.1029/1999JD900180</a>.
- 9. P. Dragic, M. Cavillon, and J. Ballato, Appl. Phys. Rev., 5, 041301, (2018). https://doi.org/10.1063/1.5048410.
- Q. Wu, Y. Qu, J. Liu, J. Yuan, S. Wan, T. Wu, X. He, B. Liu, D. Liu, Y. Ma, Y. Semenova, P. Wang, X. Xin, and G. Farrell, IEEE Sens. J., 21(11), 12734, (2020). <a href="https://doi.org/10.1109/JSEN.2020.3039912">https://doi.org/10.1109/JSEN.2020.3039912</a>.
- 11.L. Coelho, J. De Almeida, J. Santos, R. Ferreira, P. André, and D. J. P. Viegas, Plasmonics, **10**, 319 (2015). <a href="https://doi.org/10.1007/s11468-014-9811-3">https://doi.org/10.1007/s11468-014-9811-3</a>.
- 12. F. Azeem, M. R. Chaudhry, M. S. Anwar, H. A. Khan, L. Ma, and A. D. Khan, Journal of the Royal Society of New Zealand, 1, 25 (2024). https://doi.org/10.1080/03036758.2024.2395909.
- 13. Y. Guo, Y. Liang., Y. Li, B. Tian, X. Fan, Y. He, M. Liu, L. Peng, N. Tang, T. Tan, and B. Yao, Adv. Devices Instrum., 5, 41, (2024). <a href="https://doi.org/10.34133/adi.0041">https://doi.org/10.34133/adi.0041</a>.
- 14. F. Vollmer and L. Yang, Nanophotonics, 1, 267, (2012). https://doi.org/10.1515/nanoph-2012-0021.
- 15. Z. Hou, L. Chen, R. Liu, C. Zhang, X. Wu, and X. Zhang, Photon. Res., **12**, 1542, (2024). <a href="https://doi.org/10.1364/PRJ.491035">https://doi.org/10.1364/PRJ.491035</a>.
- G.A. Cavaco, R.A.M. Lameirinhas, C.P.C.V. Bernardo, J.P.N. Torres, and A. Baptista, Results Opt., 15, 100651 (2024). <a href="https://doi.org/10.1016/j.rio.2024.100651">https://doi.org/10.1016/j.rio.2024.100651</a>.
- 17. H. I. Mahdi, N. A. Bakr, and T. M. Al-Saadi, Iraqi J. Sci., **65**(8) 4313, (2024). https://doi.org/10.24996/ijs.2024.65.8.16.
- 18.L. Jaiswal, A. C. Mishra, S. Yadav, P. Lohia, D. K. Dwivedi, R. K. Yadav, U. Kulshrestha, A. M. Tighezza, and M. K. Hossain, J. Comput. Electron., 24, 39 (2025). https://doi.org/10.1007/s10825-025-02277-7.
- 19.E. Gonzalez-Valencia, E. Reyes-Vera, I. Del Villar, and P. Torres, Opt. Laser Technol., **169**, 110129 (2024). https://doi.org/10.1016/j.optlastec.2023.110129.
- L. Labrador-Páez, K. Soler-Carracedo, M. Hernández-Rodríguez, I. R. Martín, T. Carmon, and L. L. Martin, Opt. Express, 25(2), 1165 (2017). https://doi.org/10.1364/OE.25.001165.
- 21. Y.-F. Chang, Y.-C. Wang, T.-Y. Huang, M.-C. Li, S.-Y. Chen, Y.-X. Lin, L.-C. Su, and K.-J. Lin, Analytica Chimica Acta, **1341**, 343640 (2025). https://doi.org/10.1016/j.aca.2025.343640.
- 22. G. M. Jassam, S. S. Alâ, and M. F. Sultan, Iraqi J. Sci., **61**(4), 765, (2020). https://doi.org/10.24996/ijs.2020.61.4.8.
- 23. L. K. Abbas, Baghdad Sci. J., 21(8), 2730, (2024). https://doi.org/10.21123/bsj.2024.10113.
- 24. Y. Zhang, Q. Song, D. Zhao, X. Tang, Y. Zhang, Z. Liu, and L. Yuan, Opt. Laser Technol., **159**, 108955, (2023). <a href="https://doi.org/10.1016/j.optlastec.2022.108955">https://doi.org/10.1016/j.optlastec.2022.108955</a>.
- 25. W. Weng, J. Anstie, and A. Luiten, Phys. Rev. Appl., **3**, 044015 (2015). <a href="https://doi.org/10.1103/PhysRevApplied.3.044015">https://doi.org/10.1103/PhysRevApplied.3.044015</a>.
- W. Yin, Z. Shen, S. Li, Y. Cui, F. Gao, H. Hao, and X. Chen, Opt. Express, 30(18), 32162 (2022). https://doi.org/10.1364/OE.469962.
- 27. M. Zhang, W. Yang, K. Tian, J. Yu, A. Li, S. Wang, E. Lewis, G. Farrell, L. Yuan, and P. Wang, Opt. Lett., **43**(16), 3961 (2018). <a href="https://doi.org/10.1364/OL.43.003961">https://doi.org/10.1364/OL.43.003961</a>.
- 28. E. A. Hassan, A. A. Al-mfrji, and A. I. Mahmood, J. Opt., 1, 1 (2024). <a href="https://doi.org/10.1007/s12596-024-01964-1">https://doi.org/10.1007/s12596-024-01964-1</a>.

## نمذجة رياضية رنانات أنماط الرواق الهامس لاستشعار عامل الانكسار عالى الحساسية

فرح عبد الكافي لازم 1,2 وحيدر يحيى حمود 1 وأسيل أبراهيم محمود 3 أفسم الفيزياء، كلية العلوم للبنات، جامعة بغداد، بغداد، العراق 2 كلية العلوم، جامعة الكرخ للعلوم، بغداد، العراق قهيئة البحث العلمي، وزارة التعليم العالى والبحث العلمي، بغداد، العراق

#### الخلاصة

في هذه الدراسة، تم فحص ألياف SMF أحادية الوضع في بحث نظري لتأثير الوسط على نموذج رنانات أنماط الرواق الهامس FSR باستخدام برنامج MATLAB. اكتشفنا أن FSR لها علاقة عكسية مع نصف قطر الرنان وتساوي THz 0.33. سبب انخفاض قيمة FSR باستخدام برنامج MATLAB. المبب انخفاض قيمة FSR لها مرنان الكرة الدقيقة الكبير. يتم تعريف عامل Q الجيد والعالي على أنه 20.17 × 105. وُجد أن طيف الرنين يتضاءل عندما يرتفع معامل الانكسار للوسط المحيط. يتفاعل المجال المتلاشي له WGMR مع الوسط الخارجي بقوة أكبر عندما يرتفع معامل الانكسار البيئة المحيطة. تتغير الظروف الحدودية للأوضاع الرنانة بسبب هذا التفاعل، مما يرفع معامل الانكسار الفعال للأوضاع. قد يتغير تردد رنين WGMR أيضًا نتيجة للتغيرات في معامل الانكسار للوسط المحيط. التحقيق دقة استشعار عالية، يُغيّر الوسط المحيط بـ WGMR الكروي الشكل بمقدار 20.002 في نطاق 1.333 إلى 1.335 أما بالنسبة لقيمة الحساسية، فقد توصلنا إلى قيمة (-) 100.152 تيرا هرتز/وحدة RIU،

الكلمات المفتاحية: رنانات أنماط الرواق الهامس، النطاق الطيفي الحر، عامل الجودة، المجال المتلاشي، الألياف ذات الوضع الفردي.